






Generation of Vorticity Near Topography: Anticyclones in the Caribbean Sea

C. G. van der Boog^{1,2} , M. J. Molemaker³ , H. A. Dijkstra⁴ , J. D. Pietrzak¹ , and C. A. Katsman¹ 

¹Environmental Fluid Mechanics, Civil Engineering and Geosciences, Delft University of Technology, Delft, The Netherlands, ²Jet Propulsion Laboratory, California Institute of Technology, Pasadena, CA, USA, ³Department of Atmospheric and Oceanic Sciences, University of California, Los Angeles, CA, USA, ⁴Institute for Marine and Atmospheric Research Utrecht, Utrecht University, Utrecht, The Netherlands

Key Points:

- The vorticity flux into the Caribbean Sea is dominated by the local generation of vorticity near the topography of the Lesser Antilles
- North Brazil Current rings trigger local vorticity generation through increased transport, while their direct vorticity influx is limited
- This high-resolution model example suggests that vorticity generation near topography can be a significant factor in the global budget

Supporting Information:

Supporting Information may be found in the online version of this article.

Correspondence to:

C. G. van der Boog,
choog@jpl.nasa.gov

Citation:

van der Boog, C. G., Molemaker, M. J., Dijkstra, H. A., Pietrzak, J. D., & Katsman, C. A. (2022). Generation of vorticity near topography: Anticyclones in the Caribbean Sea. *Journal of Geophysical Research: Oceans*, 127, e2021JC017987. <https://doi.org/10.1029/2021JC017987>

Received 10 SEP 2021

Accepted 7 AUG 2022

© 2022 Jet Propulsion Laboratory and The Authors, California Institute of Technology. Government sponsorship acknowledged.

This is an open access article under the terms of the [Creative Commons Attribution-NonCommercial License](https://creativecommons.org/licenses/by-nc/4.0/), which permits use, distribution and reproduction in any medium, provided the original work is properly cited and is not used for commercial purposes.

Abstract Mesoscale anticyclonic eddies dominate the sea-surface height variability in the Caribbean Sea. Although it is well established that these anticyclones are formed near the eastern boundary of the Caribbean Sea, which is demarcated by the Lesser Antilles, the source of their anticyclonic vorticity remains unclear. To gain insight into this source, we analyze the fluxes of vorticity into the Caribbean at its eastern boundary using a high-resolution numerical model. We find that the anticyclonic vorticity in the eastern Caribbean Sea predominantly originates from regions where intense ocean currents flow close to the Lesser Antilles. More specifically, St. Lucia and Grenada are hotspots for vorticity generation. The local generation rate scales with the amplitude of the volume transport through the passages between these islands. This finding is in contrast with the view that anticyclonic North Brazil Current (NBC) rings in the Atlantic Ocean are the main source of anticyclonic vorticity in the eastern Caribbean Sea. Our analyses reveal that the direct contribution of the vorticity of the NBC rings is of lesser importance than the local generation. However, the collision of upstream NBC rings with the Lesser Antilles increases the volume transport through the passages into the Caribbean Sea, so that their presence indirectly leads to enhanced local production of anticyclonic vorticity. This process is an example of the importance of vorticity generation near topography, which is ubiquitous in the oceans, and expected to be important whenever currents and steep topography meet.

Plain Language Summary The surface variability in the Caribbean Sea is dominated by bodies of water that rotate in clockwise direction, referred to as anticyclonic eddies. These eddies form in the eastern part of the basin westward of the steep topography of the Lesser Antilles island arc. Because it is unclear what the source for their vorticity (i.e., what determines the tendency of the water to rotate) is, we analyze the fluxes of vorticity into the eastern Caribbean Sea. We use a numerical model with a high spatial resolution to show that two thirds of the vorticity flux is generated locally near the topography of the islands. Furthermore, the magnitude of the locally generated vorticity scales with the magnitude of the transport between the islands. In turn, this transport is regulated by the presence of anticyclonic North Brazil Current rings that collide with the Lesser Antilles. This implies that, while the direct contribution of the vorticity influx of the North Brazil Current rings is at most one third of the anticyclonic vorticity flux into the Caribbean Sea, these rings predominantly impact the vorticity influx into the Caribbean indirectly. These results highlight the importance of vorticity generation near topography for the total vorticity budget, which is expected to be important whenever currents and steep topography meet.

1. Introduction

Nearly a third of the ocean's surface is, at any given time, covered by mesoscale eddies (Gaube et al., 2019). These eddies dominate the surface variability, and they redistribute fundamental tracers along their path of propagation (Chelton et al., 2007; Fu et al., 2010; Richardson, 1983; Wunsch, 1999). Along these paths, which can be hundreds of kilometers long (Chelton et al., 2007, 2011), mesoscale eddies can collide with the steep topography of island arcs. Well-known examples of such collisions are the North Brazil Current (NBC) rings that encounter the Lesser Antilles in the Atlantic Ocean (Figure 1; e.g., Didden & Schott, 1993; Fratantoni & Richardson, 2006; Jochumsen et al., 2010) and the eddies that collide with the Kuril Islands in the Pacific Ocean (Itoh & Yasuda, 2010; Prants et al., 2016; Rabinovich et al., 2002).

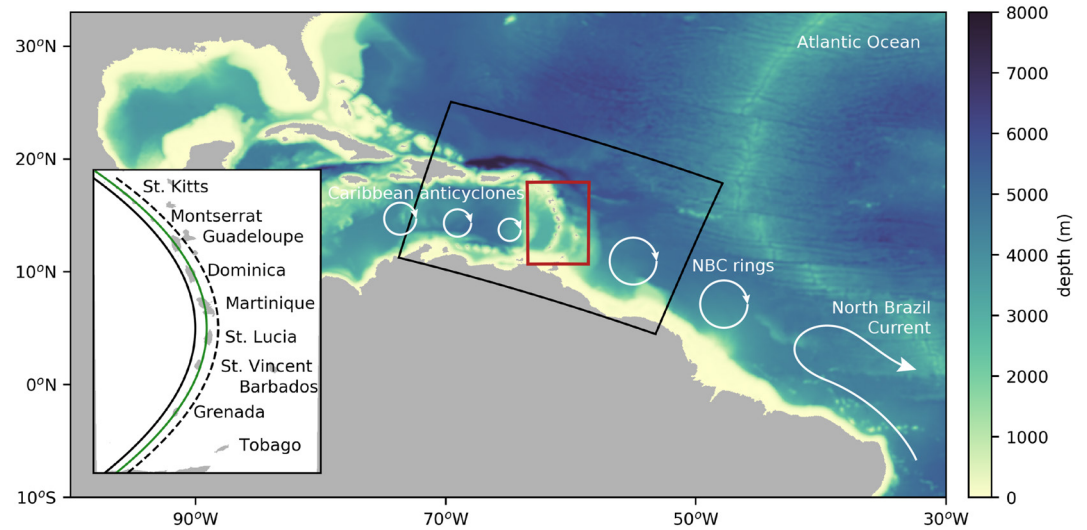


Figure 1. Map of the bathymetry of the Caribbean Sea, used in the numerical simulations. The black box indicates the domain of the first nested grid (*CS-nest*), the red box indicates the second nested grid (*LA-nest*). Typical locations and size of Caribbean anticyclones, North Brazil Current rings, and the North Brazil Current are sketched in white. The inlay, corresponding to the *LA-nest*, zooms in on the islands of the Lesser Antilles, and indicates the locations of the eastern (dashed line), middle (green line), and western (solid line) cross sections used in the analyses.

When a mesoscale eddy collides with an island arc, the eddy can either squeeze through the passages (Goni & Johns, 2001), split into smaller eddies (Cardoso et al., 2020; Richardson, 2005; Richardson & Tychensky, 1998), or completely disintegrate (Jochumsen et al., 2010). Idealized models (Duran-Matute & Fuentes, 2008; Simmons & Nof, 2002) and laboratory experiments (Cenedese et al., 2005; Tanabe & Cenedese, 2008) indicate that the response of the eddies depends on multiple factors, such as the size of the eddy, the angle of approach and the width of the gaps between the islands. While these different responses imply that not all eddies will continue their path after a collision, it is possible that filaments of their vorticity are advected downstream of the islands (Shi & Nof, 1994; Simmons & Nof, 2002). For example, Goni and Johns (2001, 2003) and Richardson (2005) suggested that vorticity filaments of NBC rings feed the formation of anticyclones directly downstream of the Lesser Antilles. However, other modeling studies (Chérubin & Richardson, 2007; Jouanno et al., 2009; van der Boog, Pietrzak, et al., 2019) suggested that a realistic eddy field in the Caribbean Sea can be obtained also without including NBC rings and hence without these filaments. Consequently, the source of the vorticity of Caribbean anticyclones still remains unclear.

Another process that may play a role is the generation of vorticity near steep topography (Deremble et al., 2016; Srinivasan et al., 2019). Multiple studies have shown that such local generation of vorticity can result in the formation of eddies (Gula et al., 2015; Jiménez et al., 2008; Johnston et al., 2019; Molemaker et al., 2015). In particular, Jiménez et al. (2008) found that the eddy generation depends on the flow velocities near the topography. Despite that these studies all focused on other regions than the Lesser Antilles, this type of vorticity generation is generic and expected to be relevant here, because the topography is steep and the volume transport through the narrow passages is large (Johns et al., 2002). It is therefore necessary to account for this process when studying the potential link between NBC rings in the Atlantic Ocean and anticyclones in the Caribbean Sea.

Here, we study the vorticity fluxes in a region encompassing the Lesser Antilles and use those to quantify and contrast both the net generation of vorticity in this region and the net advection of vorticity through this region from the Atlantic Ocean into the Caribbean Sea. This allows us to gain insight into the origin of the vorticity sources that feed the generation of Caribbean anticyclones. For this, we use a high-resolution regional model to accurately represent the eastern Caribbean Sea (Sections 2 and 3). First, we quantify both the time-averaged and the time-varying vorticity fluxes near the Lesser Antilles to assess the relative contribution of the advected and locally generated vorticity (Section 4). Moreover, to evaluate the contribution of the anticyclonic vorticity of NBC rings to the anticyclonic vorticity in the eastern Caribbean Sea, we study an example of a collision event of one NBC ring with the Lesser Antilles in detail in Section 5. The implications of our main result, namely that the

Table 1
Grid Settings of Simulations Used in This Study: The Nominal Horizontal Grid Resolution (Δx , Δy) and Number of Vertical Levels (N)

domain	Δx , Δy (km)	N	Δz_{\min} (m)	Δz_{\max} (m)
Atlantic Ocean (<i>parent</i>)	7	50	5.2	106.8
Caribbean Sea (<i>CS-nest</i>)	2	100	2.7	42.2
Lesser Antilles (<i>LA-nest</i>)	0.7	100	2.7	42.2

Note. The minimum and maximum vertical grid size (Δz) in a water column of 2,000 m are shown in the right column.

bulk of the vorticity flux into the eastern Caribbean Sea is generated in the vicinity of the Lesser Antilles, are discussed in Section 6.

2. Model Configuration and Methods

2.1. Model Configuration

We performed a simulation of the eastern Caribbean Sea using the Regional Oceanic Modeling System (ROMS, Shchepetkin & McWilliams, 2005). The ROMS model uses terrain-following σ -coordinates to solve the primitive equations with a full equation of state (Shchepetkin & McWilliams, 2011). We applied a one-way nesting procedure to force higher resolution regional computational domains (see Mason et al., 2010). As a parent simulation, we

used the simulation with a nominal resolution of 7 km that covers most of the Atlantic Ocean (Table 1) described in Mason et al. (2011). We refer to that paper for further details. The first nested grid covered the eastern part of the Caribbean Sea and had a nominal resolution of 2 km (*CS-nest*, black box in Figure 1 and Table 1). This simulation was run for 720 days (2 model years). The second nested grid, referred to as *LA-nest*, was located inside the *CS-nest* around the Lesser Antilles (red box in Figure 1), and had a nominal horizontal resolution of 700 m. This configuration was run for 54 days to study a single collision event of an NBC ring with the Lesser Antilles in detail (Table 1).

The bathymetry of both nests was constructed with the SRTM30-plus data set (http://www.topex.ucsd.edu/WWW_html/srtm30_plus.html). The minimum depth was restricted to 5 m, and land areas were masked using the coastlines obtained from the GSHHS data set (<http://www.soest.hawaii.edu/pwessel/gshhg/>). At these land points, the velocities were set to zero, which is equivalent to applying a no-slip boundary condition.

It is well known that in models with terrain-following coordinates pressure-gradient errors arise near steep topography, such as near the Lesser Antilles. To mitigate these pressure-gradient errors that are associated with the terrain-following coordinates of the ROMS, the raw bathymetry data was adjusted. First, the raw bathymetry data was smoothed with a Gaussian smoothing kernel that had a width of 6 times the horizontal grid resolution. Next, the steepness of the slopes was limited by setting the slope-parameter, r , which performs a logarithmic smoothing to the topography, to $r = 0.2$ (for further details see Lemarié et al., 2012). As a final step, a stretching procedure was applied to the grid. This stretching provides a higher resolution near the surface and bottom such that the surface and bottom boundary layers were better resolved (Table 1). Note that this stretching allows for the representation of a bottom boundary layer, which diminishes the artificial injection of vorticity at these locations.

Besides this adjustment of the bathymetry, the numerical schemes implemented in the ROMS are designed to mitigate the pressure-gradient error as well (detailed description in Shchepetkin & McWilliams, 2003). In short, two important steps are taken in the numerics. First, the density and depth are treated as continuously differentiable polynomial functions in the computation of the pressure-gradient force. In contrast to previous methods with a second order accuracy, this results in a fourth-order accurate function where special attention is paid to spatially nonuniform grids. Second, Shchepetkin and McWilliams (2003) showed that disregarding the compressibility of sea water results in significant errors that can even be larger than the classical pressure-gradient errors due to the hydrostatic inconsistency associated with the terrain-following grids. These errors are mitigated by accounting for the compressibility of sea water (i.e., the model is non-Boussinesq).

At the surface, a repeating climatological normal year forcing similar to that applied by Lemarié et al. (2012) was used. The daily wind stresses for this normal year forcing were computed using the QuikSCAT-based daily product of scatterometer wind stresses (Risien & Chelton, 2008), which were corrected for the effect of surface currents on the wind stress (Lemarié et al., 2012). Climatological monthly averaged surface heat fluxes were constructed with CORE (Large & Yeager, 2009). We applied an idealized diurnal cycle to the incoming short-wave radiation. Note that, although this simplified diurnal cycle implies that the influence of extreme events on the vorticity is not taken into account, we argue that it is sufficient to study the role of topography on the production of vorticity. The climatological monthly averaged precipitation and evaporation were obtained from HOAPS (Andersson et al., 2010). The outflow of rivers was implemented using climatological discharges obtained from Dai and Trenberth (2002). Different from Lemarié et al. (2012), the discharge of each river was prescribed by means of an array of point sources near the river mouth. At these point sources, monthly discharges were

prescribed over the full water column with a salinity of 1 psu and an idealized seasonally varying temperature that varied with an amplitude of 1 °C around a mean of 28 °C. The velocity imposed at the river outflow was scaled with the total area of the outflow to get a volume transport that matched the observed discharges.

At the lateral boundaries of both nested grids, a sponge layer with a width of 1/12 of the domain size was defined to smoothly connect the nested-grid solutions to the prescribed boundary conditions. This sponge layer was implemented as an explicit lateral viscosity that increased from 0 near the interior to 5 m² s⁻¹ and 0.1 m² s⁻¹ at the boundary of the *CS-nest* and *LA-nest*, respectively. The explicit lateral viscosity is set to 0 m² s⁻¹ in the interior of both nests. Horizontal viscosity was implicitly parameterized by using a third-order horizontal upstream-biased advection scheme and a vertical semiimplicit advection scheme (for further details, see Shchepetkin, 2015). We applied the K-profile parameterization (KPP, Large et al., 1994) to parameterize the vertical mixing of tracers and momentum. We parameterized bottom friction, using the logarithmic law with a roughness length of 0.01 m. To limit spurious diapycnal mixing, isoneutral diffusion was applied in both nested grids (Lemarié et al., 2012).

2.2. Methods

For both nests, snapshots of the velocity, temperature, salinity, and sea-surface height anomalies were saved every 6 hr. The temperature and salinity fields were converted to conservative temperature and absolute salinity, respectively, using the TEOS-10 software (McDougall & Barker, 2011) to allow for comparison with data from the World Ocean Atlas 2018 (WOA2018, Locarnini et al., 2019; Zweng et al., 2019). To validate the magnitude of the volume transports into the eastern Caribbean Sea against observations from Johns et al. (2002) and Kirchner et al. (2008), we defined a cross section through the Lesser Antilles (green line in the inlay of Figure 1) and computed the volume transports perpendicular to this cross section.

To determine the sources of the anticyclonic vorticity in the eastern Caribbean Sea, we first computed the relative vorticity from the 6-hourly snapshots. The vertical component of the relative vorticity, simply referred to as vorticity in the remainder of this study, was defined as:

$$\zeta = \frac{\partial v}{\partial x} - \frac{\partial u}{\partial y}, \quad (1)$$

where u and v are the velocities in zonal (x direction) and meridional (y direction) direction, respectively. The terms on the right-hand side were computed from snapshots of the three-dimensional velocities fields on the terrain-following coordinates:

$$\left[\frac{\partial v}{\partial x} \right]_z = \left[\frac{\partial v}{\partial x} \right]_\sigma - \left[\frac{\partial z}{\partial x} \right]_\sigma \frac{\partial v}{\partial z} \quad (2a)$$

$$\left[\frac{\partial u}{\partial y} \right]_z = \left[\frac{\partial u}{\partial y} \right]_\sigma - \left[\frac{\partial z}{\partial y} \right]_\sigma \frac{\partial u}{\partial z} \quad (2b)$$

where the subscripts z and σ indicate the direction along horizontal surfaces and along the terrain-following surfaces, respectively. In these computations, we ignored sea level variations.

Next, we define the budget for the vorticity, needed to quantify the generation of vorticity near the Lesser Antilles, as

$$\frac{D\zeta}{Dt} = -\beta w + (\zeta + f) \frac{\partial w}{\partial z} + \left(\frac{\partial u}{\partial z} \frac{\partial w}{\partial y} - \frac{\partial v}{\partial z} \frac{\partial w}{\partial x} \right) + \rho^{-2} \left(\frac{\partial \rho}{\partial x} \frac{\partial p}{\partial y} - \frac{\partial \rho}{\partial y} \frac{\partial p}{\partial x} \right) + \left(\frac{\partial F_y}{\partial x} - \frac{\partial F_x}{\partial y} \right) \equiv S_\zeta \quad (3)$$

where β corresponds to the meridional variation of planetary vorticity ($\beta = \frac{\partial f}{\partial y} = \frac{\partial 2\Omega \sin \phi}{\partial y}$, where ϕ corresponds the latitude and Ω to the rotation rate of the Earth), w to the vertical velocity, ρ to the sea water density, p to the pressure. F_x and F_y correspond to forcing terms that can act as additional sources and sinks of vorticity. For simplicity, we define S_ζ as the sum of the terms on the right-hand side of Equation 3.

We performed the analyses on a control volume around the Lesser Antilles. A three-dimensional schematic of this control volume is shown in Figure 2. The dashed and solid line in the inlay of Figure 1 outline the horizontal boundaries of this control volume. Its western and eastern edges are 0.5° apart, and encompass the Lesser

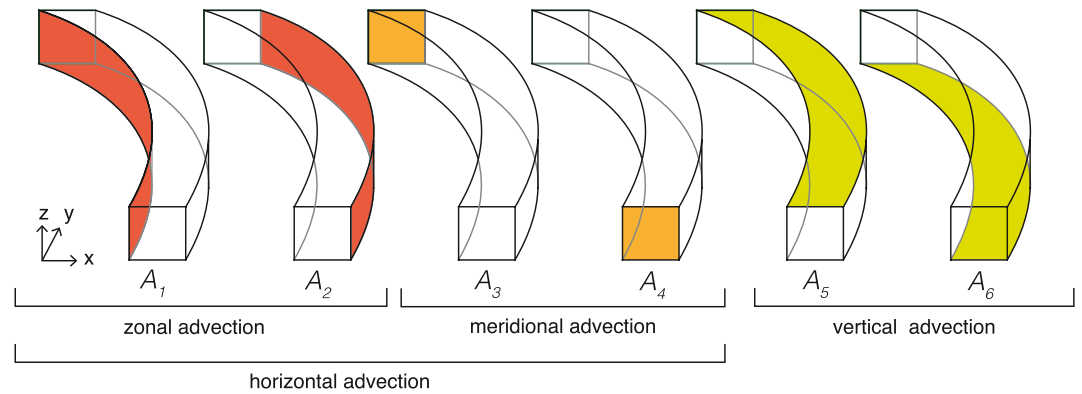


Figure 2. Schematic of the control volume around the Lesser Antilles defined to calculate the vorticity budget, indicating the bounding surfaces in zonal, meridional, and vertical direction. The meridional boundaries of the control volume are located between 10.6°N and 17.9°N; its zonal boundaries are 0.5° apart and outlined by the dashed and solid line in the inlay of Figure 1. It extends from the surface to 300 m depth.

Antilles. Its northern and southern edges are located between 10.6°N and 17.9°N. By choosing these horizontal boundaries some distance away from the islands, we circumvent calculating the complex and potentially noisy local vorticity fluxes near their complex and steep bathymetry in detail. Instead, we focus on the net vorticity generation within the control volume and contrast this with net vorticity advection through the volume. In the vertical, the control volume extends from the surface to 300 m depth. This depth was chosen because the bulk of the transport, and thus of the fluxes, is found in this depth range. Furthermore, we defined u_n as the velocity perpendicular to the sides of the control volume, where the velocities directed toward the Caribbean (A_1, A_2), in southward direction (A_3, A_4) and upward (A_5, A_6) were defined as positive.

The vorticity budget over the control volume can be expressed as the combination of the net advection over all edges of the control volume and the net effect of generation and dissipation of vorticity inside the control volume:

$$\int_V \frac{\partial \zeta}{\partial t} dV + \underbrace{\sum_{j=2,3,6} \int_{A_j} u_n \zeta dA_j}_{\text{advection into control volume}} - \underbrace{\sum_{i=1,4,5} \int_{A_i} u_n \zeta dA_i}_{\text{advection out of control volume}} = \underbrace{\int_V S_\zeta dV}_{\text{net sources/sinks}} \quad (4)$$

where i and j indicate the faces of the control volume (Figure 2).

The net horizontal advection of vorticity into the Caribbean Sea is the flux across the western face of the control volume (A_1), that from the Atlantic Ocean into the control volume is the flux across its eastern face (A_2 , Figure 2). In Section 4, we will show that the vorticity fluxes through these two surfaces A_1 and A_2 are much larger than the meridional advection (through A_3) and vertical advection (through A_6). Moreover, the vorticity fluxes through A_4 and A_5 are by construction zero, as they are on land and at the surface, respectively. Consequently, the difference between the advection of vorticity into the Caribbean across surface A_1 and the advection from the Atlantic Ocean across surface A_2 can be used as a measure for the net generation and dissipation of vorticity in the vicinity of the Lesser Antilles:

$$\underbrace{\int_{A_2} u_n \zeta dA_2}_{\text{advection from Atlantic Ocean}} - \underbrace{\int_{A_1} u_n \zeta dA_1}_{\text{advection into Caribbean Sea}} \approx \underbrace{\int_V S_\zeta dV}_{\text{net generation / dissipation}} \quad (5)$$

where the temporal change in vorticity (first term on the left-hand side of Equation 4) can be neglected when all terms are time-averaged over time periods longer than the advection time scales.

The right-hand side of Equation 5 represents the net effect of all sources and sinks of vorticity inside the control volume. For example, vorticity can be generated by vortex stretching and tilting, and the presence of bottom friction near the steep topography induces the generation of vorticity in the bottom boundary layer. The latter is expected to considerably contribute to the vorticity budget in this region. However, as the main aim of this study

Table 2
2-Year Averaged Volume Transports in Sv ($1 \text{ Sv} = 10^6 \text{ m}^3 \text{ s}^{-1}$) Through the Passages Between the Lesser Antilles in the Model (CS-nest, Second Column) and in Available Observations (Johns et al., 2002; Kirchner et al., 2008)

Section	CS-nest	Johns et al. (2002)	Kirchner et al. (2008)
Montserrat—St. Kitts	0.30 ± 0.02		
Guadeloupe—Montserrat	0.83 ± 0.03	1.1 ± 1.1	
Dominica—Guadeloupe	1.43 ± 0.03	1.6 ± 1.2	0.7 ± 0.5
Martinique—Dominica	1.04 ± 0.06	1.6 ± 1.2	1.6 ± 0.5
St. Lucia—Martinique	2.74 ± 0.04	1.5 ± 2.4	1.2 ± 0.5
St. Vincent—St. Lucia	3.62 ± 0.05	2.9 ± 2.2	3.6 ± 0.5
Grenada—St. Vincent	1.03 ± 0.01		
Venezuela—Grenada	4.60 ± 0.06	5.7 ± 2.4	
66°W	21.12 ± 0.54	18.4 ± 4.7	

Note. Standard errors of the mean are indicated at the cross section along the Lesser Antilles (the green line in Figure 1). Positive numbers correspond to transports into the Caribbean Sea.

is to quantify the net generation of vorticity near the Lesser Antilles and compare it to the net advection of vorticity from the Atlantic Ocean, we leave a detailed analysis of these different local sources and sinks of vorticity for further research and focus here solely on the net effect of vorticity generation and dissipation within the control volume.

Whenever the advection of vorticity into the Caribbean exceeds the advection of vorticity from the Atlantic (left-hand side of Equation 5 > 0), the anticyclonic vorticity inside the control volume has decreased and/or the cyclonic vorticity has increased. To distinguish these, we used a Heaviside function to define separate expressions for the net generation/dissipation of anticyclonic vorticity (G_{ac}) and of cyclonic vorticity (G_{cy}):

$$G_{ac} \approx \int_{A_2} u_n |\zeta| H(\zeta < 0) dA_2 - \int_{A_1} u_n |\zeta| H(\zeta < 0) dA_1 \quad (6a)$$

$$G_{cy} \approx \underbrace{\int_{A_2} u_n |\zeta| H(\zeta > 0) dA_2}_{\text{advection from Atlantic Ocean}} - \underbrace{\int_{A_1} u_n |\zeta| H(\zeta > 0) dA_1}_{\text{advection into Caribbean Sea}} \quad (6b)$$

Before we use these methods to analyze the advection of vorticity from the Atlantic versus the generation of vorticity near the Lesser Antilles (Sections 4 and 5), we assess the model in Section 3.

3. Model Validation

3.1. Mean Flow

The mean flow in the Caribbean Sea enters the basin through the Lesser Antilles (Johns et al., 2002). In line with observations (Johns et al., 2002; Kirchner et al., 2008), the bulk of the modeled flow enters the basin through the passages between the southern islands (Table 2). The modeled volume transport through all passages adds up to $21.12 \pm 0.54 \text{ Sv}$ at 66°W, which is in line with to the volume transport of $18.4 \pm 4.7 \text{ Sv}$ estimated from observations (Johns et al., 2002). Of this transport, 56% occurs in the upper 300 m of the water column.

Also in line with observations (Johns et al., 2002; Kirchner et al., 2008), we find that the flow into the Caribbean is highly variable (Table 2), which is partly driven by the 2–7 NBC rings that propagate toward the Caribbean Sea each year (Goni & Johns, 2003; Mélice & Arnault, 2017; Mertens et al., 2009). More specifically, Mertens et al. (2009) showed that, before NBC rings reach the Lesser Antilles, they decrease the volume transport into the Caribbean, while they increase the volume transport during the actual collision with the islands.

3.2. Caribbean Anticyclones

To evaluate the ability of the model to simulate the eddy field, we analyze the properties of selected Caribbean anticyclones and their vertical structure and compare these to available observations, focusing on in the eastern Caribbean Sea. Caribbean anticyclones are known to dominate the sea-surface variability in the Caribbean basin (e.g., Centurioni & Niiler, 2003; Richardson, 2005), and surface drifter data indicates that approximately 4–8 anticyclones are formed each year (Richardson, 2005). Even though exact correspondence between the simulation and satellite altimetry is not to be expected, since the model uses repeated climatological forcing (see Section 2), the model results are in line with these observations. An automated eddy tracker (Mason et al., 2014) and visual inspection of the sea level anomalies indicate that 13 anticyclones are formed in the vicinity of the Lesser Antilles during the 2-year simulation.

Further inspection of cross sections of these anticyclones in the model indicates that, based on their vertical structure, two types of Caribbean anticyclones may be distinguished: shallow and deep anticyclones. The shallow anticyclones have a pronounced surface-intensified character where the strongest velocities are confined to approximately the upper 200 m of the water column. The deep anticyclones also display strong velocities below

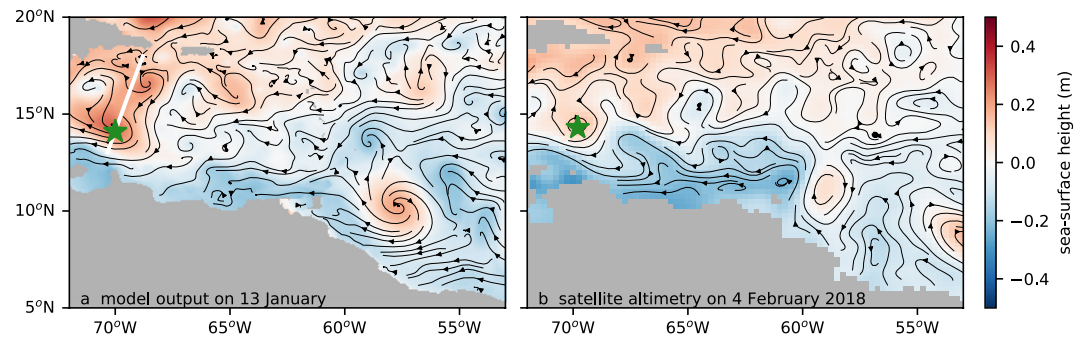


Figure 3. Sea-surface height (a) in the *CS-nest* simulation on 13 January and (b) from satellite altimetry on 4 February 2018. Streamlines of the flow are indicated with black curves. Green stars highlight the location of anticyclones discussed in Section 3.2. The white line indicates the location of the cross sections depicted in Figure 4. The sea-surface height from satellite altimetry in (b) is computed from multimission altimeter satellite gridded sea-surface heights, downloaded from the Copernicus Marine Environment Monitoring Service (<http://marine.copernicus.eu>).

this depth. In situ observations of the vertical structure of Caribbean anticyclones are scarce, but also contain examples of both these types.

The modeled shallow anticyclones have a similar velocity structure as the eddy survey performed in February 2019 discussed in van der Boog, de Jong et al. (2019), and hence we choose a simulated shallow anticyclone present in the model at the same time of the year and near the location of this hydrographic survey for comparison to these observations (central Caribbean; eddies indicated by green stars in Figure 3). Both anticyclones are intensified at the surface (Figures 4a and 4b) and have a strong velocity shear directly below the main thermocline at 100–200 m depth (Figures 4c and 4d). Furthermore, the mixed-layer depths of the modeled anticyclone and of the observed anticyclone are about the same depth (MLD = 80 m), and the mixed layers in both anticyclones are limited by the halocline (orange lines in Figures 4e and 4f). This is typical for the Caribbean Sea in winter, and indicates the presence of a barrier layer, which is defined as the layer between the halocline and thermocline (de

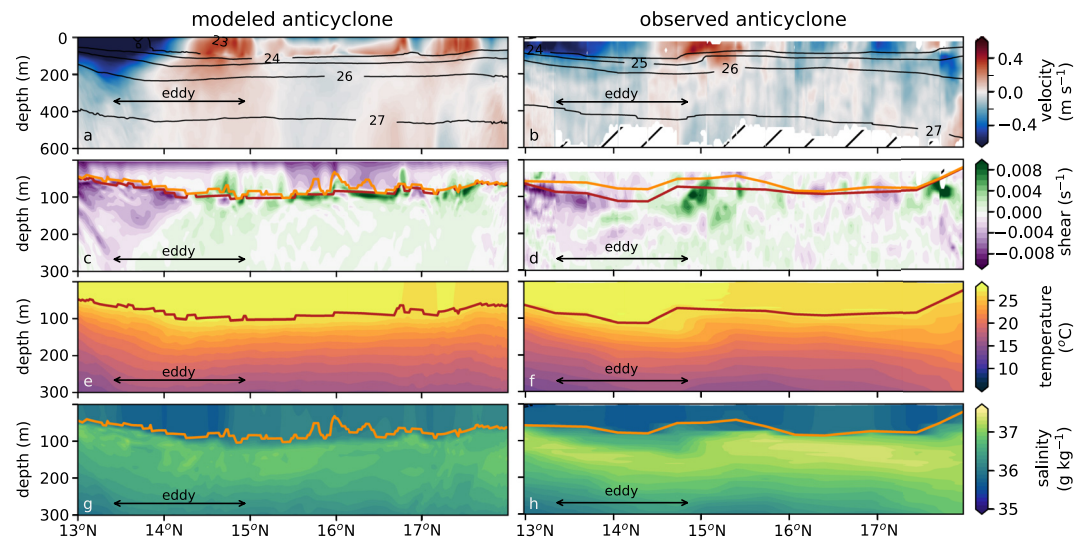


Figure 4. Comparison of the characteristics of a (left) modeled and (right) observed shallow anticyclone in the Caribbean Sea in winter, by means of cross sections of the (a, b) velocity perpendicular to the cross section (m s^{-1}), (c, d) vertical shear of this velocity (s^{-1}), (e, f) conservative temperature ($^{\circ}\text{C}$), and (g, h) absolute salinity (g kg^{-1}) of (left column) a modeled anticyclone and of (right column) the observed anticyclone as described by van der Boog, de Jong et al. (2019). The modeled anticyclone was present at 13 January; the surveyed anticyclone was observed on 4 February 2018 by (van der Boog, de Jong et al., 2019). Contour lines in panel (a, b) show the isopycnals. The thermocline and halocline, indicated with the red and orange curve respectively, were computed following Mignot et al. (2012).

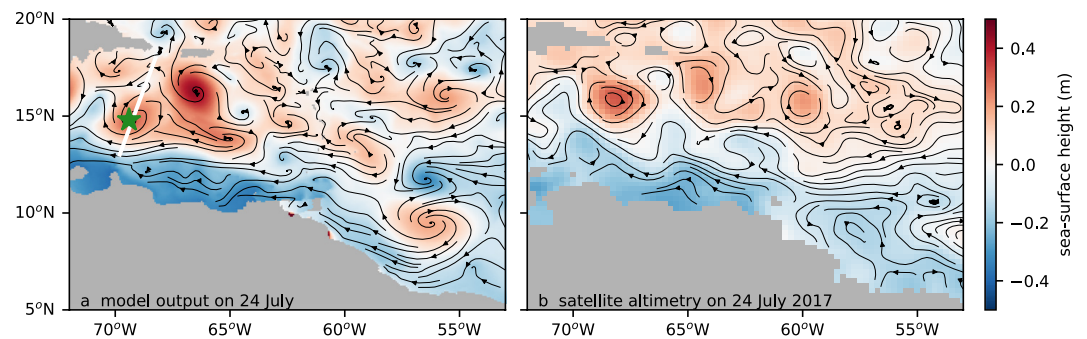


Figure 5. Sea-surface height (m) in the (a) *CS-nest* on 24 July of year 6 and (b) from satellite altimetry on 24 July 2017. Streamlines of the flow are indicated with black curves. The green star highlights the location of anticyclones discussed in Section 3.2. The white line indicates location of cross section of Figure 6. The sea-surface height from satellite altimetry is computed from multimission altimeter satellite gridded sea-surface heights, downloaded from the Copernicus Marine Environment Monitoring Service (<http://marine.copernicus.eu>).

Boyer Montégut et al., 2004; Mignot et al., 2007; Rudzin et al., 2017). The fact that the model captures such a barrier layer suggests that it has a realistic representation of the mixed-layer dynamics.

The modeled deep anticyclones appear to have a vertical structure corresponding to that of the eddy observed by Rudzin et al. (2017) in summer. They performed upper-ocean measurements of a Caribbean anticyclone and concluded that this example was a coherent vortex down to at least 500 m depth. Therefore, we compare snapshots of sea-surface height from the simulation (Figure 5a) and from satellite altimetry in the season these observations were taken (Figure 5b). For comparison of the vertical structure, we again choose a simulated eddy in the same region at the same time (green star in Figure 5a). The vertical structure of the modeled deep anticyclone is shown in Figure 6. Strong velocities are found below the thermocline (red line in Figure 6b). The structure of the vertical shear indicates that this anticyclone extends down to roughly 350–400 m (Figure 6b). This is in line with the observation of Rudzin et al. (2017).

A final interesting comparison to make is between the magnitude of the sea-surface height gradients in winter and summer between model and observations. Sea-surface height gradients are usually stronger in summer than in winter, and as a result Caribbean anticyclones tend to be more energetic in summer than in winter (Jouanno et al., 2012). In the simulations, the sea-surface height gradients indeed show that characteristic, as can already be seen from the snapshots (Figures 3a and 5a). This can also be quantified by calculating the median sea-surface height gradient (∂SLA_{median}) from Figures 3 and 5. In summer, $\partial SLA_{median}^{summer}$ is 1.23 mm km^{-1} , and in winter $\partial SLA_{median}^{winter}$ is 0.92 mm km^{-1} . A comparison to a sea-surface height field obtained from satellite altimetry confirms

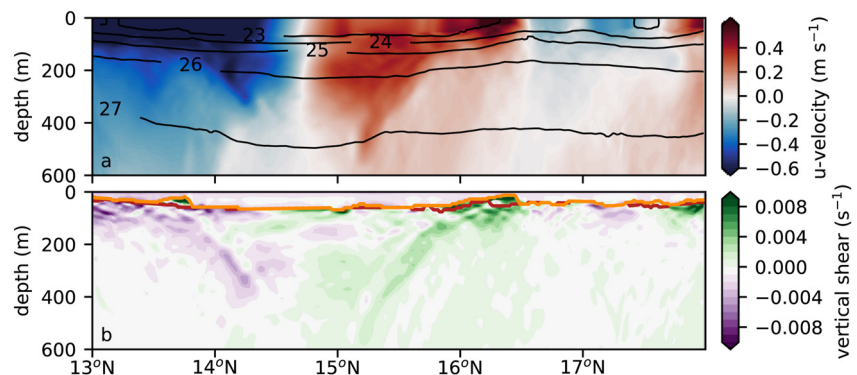


Figure 6. Characteristics of a modeled deep anticyclone in summer, by means of cross sections of the (a) u-component of the velocity (m s^{-1}), (b) vertical shear of the u-component of the velocity (s^{-1}), taken at the location indicated in Figure 5 on 24 July year 6. Contour lines in panel (a) show the isopycnals. The thermocline and halocline, indicated with the red and orange line respectively, were computed following Mignot et al. (2012). Note that the vertical axis of Figure 6b extends deeper than in Figures 4c and 4d.

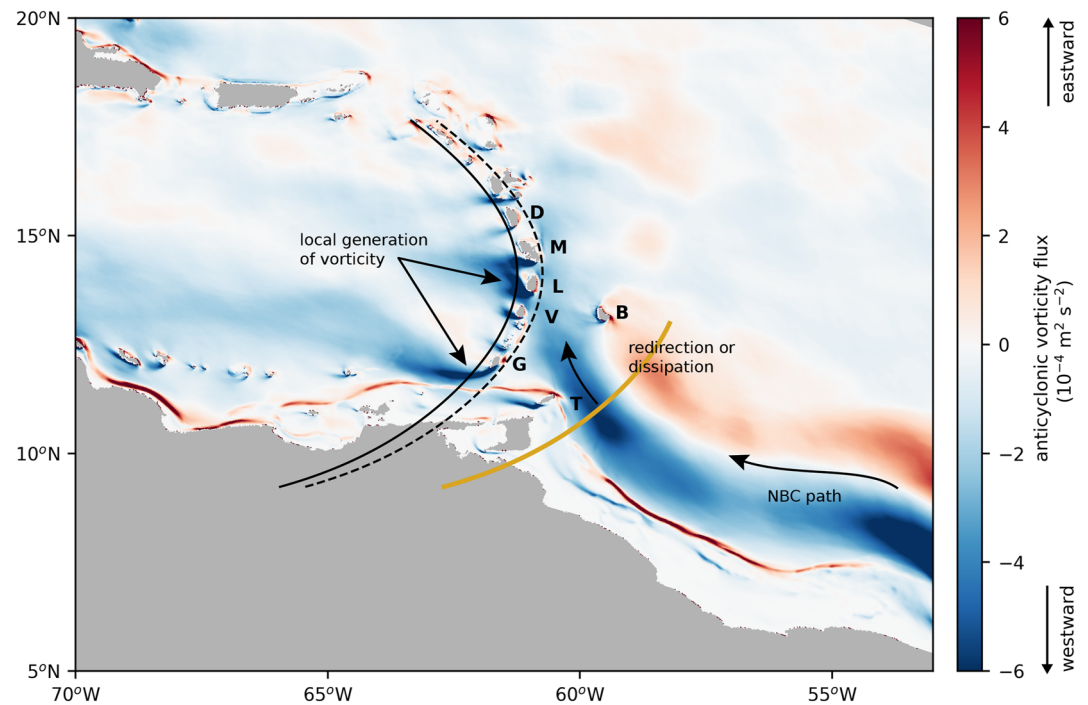


Figure 7. Zonal component of the anticyclonic vorticity flux integrated over the upper 300 m of the water column and averaged over 2 years model data from *CS-nest*. Negative values correspond to a flux in westward direction. Dashed and solid lines indicate the locations of the cross sections east and west of the Lesser Antilles, respectively. Letters are placed east of the islands to indicate their location: D = Dominica, M = Martinique, L = St. Lucia, V = St. Vincent, G = Grenada, T = Tobago, B = Barbados. The yellow curve indicates the location of the cross section along which the maximum sea level anomaly is obtained that is used to gain insight into the passage of North Brazil Current (NBC) rings in Section 4.2 (Figure 9d).

that this is in line with observations (compare Figures 3b and 5b), where $\partial\text{SLA}_{\text{median}}^{\text{summer}} = 0.58 \text{ mm km}^{-1}$ is also larger than $\partial\text{SLA}_{\text{median}}^{\text{winter}} = 0.48 \text{ mm km}^{-1}$. Note that the values obtained from the satellite altimetry are smaller than those obtained from the model simulations due to the coarser horizontal resolution of the gridded altimetry product.

In summary, this comparison between modeled and observed vertical structure of Caribbean anticyclones indicates that the model generates anticyclones with varying characteristics, in particular with respect to their vertical structure, in line with the limited data that is available. As it generates both shallow anticyclones like the one observed by van der Boog, de Jong et al. (2019) and deeper-reaching anticyclones resembling the eddy observed by Rudzin et al. (2017), the model seems capable of capturing this diversity.

4. Advective Vorticity Flux Into the Caribbean Sea

4.1. Mean Fluxes

To quantify the fluxes of anticyclonic vorticity into the eastern Caribbean Sea, we compute the 2-year averaged zonal flux of anticyclonic vorticity integrated over the upper 300 m of the water column $\int u\zeta dz$ (Figure 7; negative values correspond to a flux in westward direction). This figure highlights a remote and a local source of vorticity: the advection of vorticity from the Atlantic Ocean, and the generation of vorticity near the Lesser Antilles. The advection of anticyclonic vorticity includes the westward propagation of anticyclonic NBC rings, and is visible as a coherent (i.e., westward) flux of anticyclonic vorticity path from the Atlantic toward the Lesser Antilles (Figure 7). The magnitude of the flux decreases between Tobago (T) and Barbados (B), which indicates that part of this anticyclonic vorticity flux is dissipated or redirected in meridional direction there. West of the Lesser Antilles, large fluxes of anticyclonic vorticity into the Caribbean (dark blue patches in Figure 7) are seen that are not connected to those occurring in the Atlantic Ocean. These have the largest magnitude near the southern

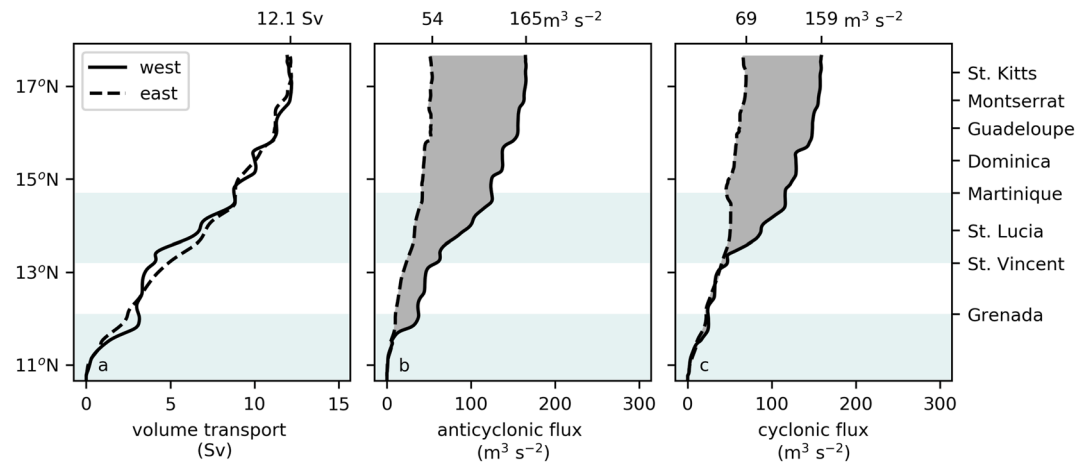


Figure 8. Two-year averaged (a) transport, (b) anticyclonic vorticity flux, and (c) cyclonic vorticity flux at the Lesser Antilles, integrated over the upper 300 m of the water column and cumulative along latitude. The dashed and solid lines correspond to the fluxes at the eastern and western edges of the control volume defined in Figures 1 and 2, respectively. The gray shaded area corresponds to the relative vorticity that is generated locally between the cross sections. The blue shading indicates passages that display enhanced generation of vorticity. Data are from *CS-nest*.

boundaries of the islands, which is indicative for the local generation of anticyclonic vorticity. In contrast, local generation of cyclonic vorticity appears on the northern flanks of the islands (Figure 1 in the Supporting Information S1). Especially near Grenada (G) and St. Lucia (L), we find a clear signal that anticyclonic vorticity is generated locally (arrows in Figure 7).

Next, we quantify the relative contribution of both sources of vorticity to the total influx of vorticity into the Caribbean Sea, from the vorticity fluxes through area A_1 and A_2 of the control volume (Figure 2). Recall that these fluxes were calculated perpendicular to these surfaces and thus contain the contributions of both zonal and meridional advection of vorticity. The difference in these vorticity fluxes can be used as a measure for the generation of the vorticity within the control volume, because the volume transport through the eastern and western cross section is similar (Figure 8a). West of the Lesser Antilles, a total section-integrated flux of $165 \text{ m}^3 \text{ s}^{-2}$ of anticyclonic vorticity is transported into the Caribbean Sea (solid line in Figure 8b). Of this flux, $54 \text{ m}^3 \text{ s}^{-2}$ can be attributed to the advection of anticyclonic vorticity toward the Lesser Antilles from the east (dashed line in Figure 8b). The difference of $111 \text{ m}^3 \text{ s}^{-2}$ between these cross sections reflects the vorticity advected through the bottom of the control volume, through the northern face of the control volume and the local generation of vorticity between the cross sections (G_{ac} in Equation 6a, gray shading in Figure 7b). This comprises 67% of the total anticyclonic vorticity flux into the eastern Caribbean Sea. The anticyclonic vorticity advected through the bottom of the control volume and the northern face of the control volume is $-1 \text{ m}^3 \text{ s}^{-2}$ and $1.8 \text{ m}^3 \text{ s}^{-2}$, respectively. Consequently, the difference in vorticity flux through the eastern and western cross section can be attributed to the local generation of vorticity between the cross sections A_1 and A_2 of the control volume. This is much larger than the contribution of the vorticity that is advected from the Atlantic Ocean, which contains the vorticity contribution of NBC rings (33%).

Similar to what we find for the anticyclonic vorticity flux, the cyclonic vorticity flux into the eastern Caribbean Sea is also dominated by the local generation of vorticity near the Lesser Antilles (G_{cy} in Equation 6a, gray shading in Figure 8c). The magnitude of the cyclonic vorticity flux west of the Lesser Antilles is $159 \text{ m}^3 \text{ s}^{-2}$, of which $69 \text{ m}^3 \text{ s}^{-2}$ is attributed to advection of cyclonic vorticity from the Atlantic Ocean (solid and dashed lines in Figure 8c, respectively). This implies that 57% of the cyclonic vorticity flowing into the Caribbean Sea is generated between the two cross sections A_1 and A_2 .

Besides quantifying the relative contributions of the generation of vorticity near the Lesser Antilles and the vorticity advected from the Atlantic Ocean, Figure 8 also shows that the generation of vorticity varies latitudinally as is reflected by a strong difference in meridional gradients between the cross sections. From Figure 8b, two regions with enhanced local generation of anticyclonic vorticity can be identified (blue shading): south of Grenada and between St. Vincent and Martinique. In contrast, at latitudes where the meridional gradients in the

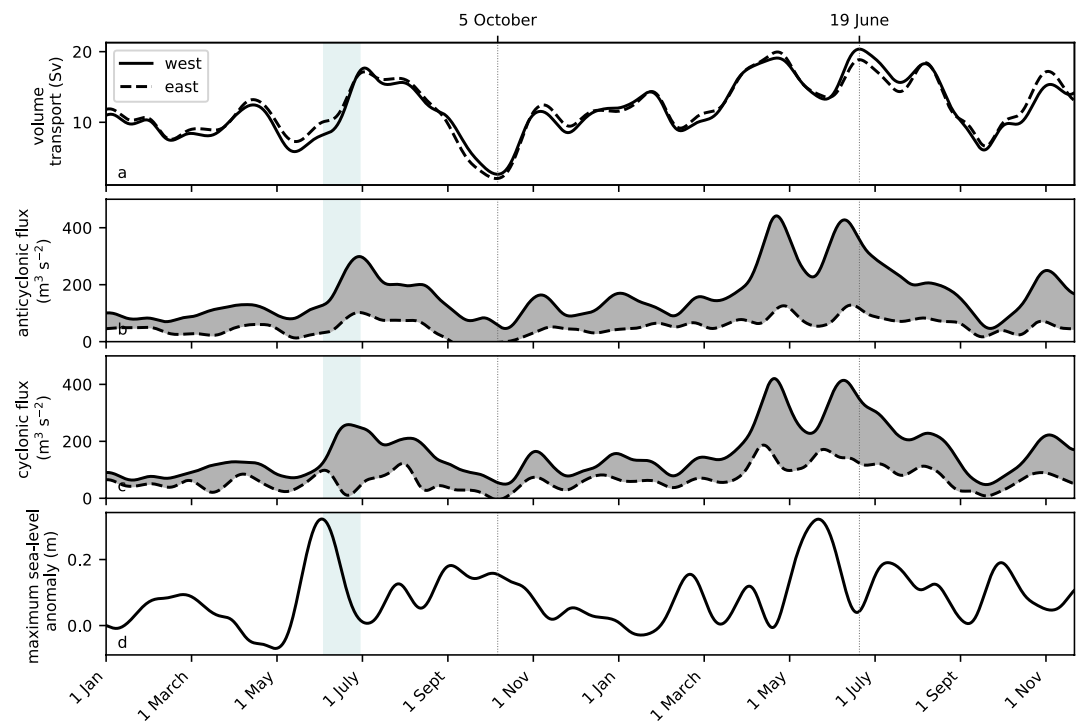


Figure 9. Total (a) volume transport (b) anticyclonic vorticity flux, and (c) cyclonic vorticity flux at the Lesser Antilles integrated along the eastern (dashed lines) and western (black solid line) cross section (Figure 1) integrated over the upper 300 m of the water column. The gray shaded area indicates the generation of vorticity between the cross sections. (d) Maximum sea level anomaly between Barbados and Tobago along the yellow curve in Figure 7. The blue shading indicates the collision of a North Brazil Current (NBC) ring with the Lesser Antilles that is described in Section 5. The data are smoothed with a Hanning function with a window of 30 days. 5 October and 19 June indicate the times of minimum and maximum volume transport through the Lesser Antilles.

eastern cross section are similar to the western cross section, the vorticity flux into the Caribbean Sea is predominantly advected from the Atlantic Ocean. This occurs, for example, between Grenada and St. Vincent and north of Martinique.

Following Jiménez et al. (2008), we expect that the magnitude of the vorticity generation is related to the flow speed and thus to the magnitude of the volume transport through the passages. Indeed, passages with a strong volume transport also have enhanced generation of anticyclonic vorticity (blue shading in Figures 8a and 8b). For example, the passages south of Grenada and between St. Vincent and Martinique contain 67% of the total volume transport into the eastern Caribbean Sea, and approximately 69% of the anticyclonic vorticity is generated here. The volume transport through the other passages (between Grenada and St. Vincent and north of Martinique), where little anticyclonic vorticity is generated, is much weaker (4.1 Sv, Figure 8a). Overall, these findings suggest that the bulk of the anticyclonic vorticity that enters the Caribbean Sea is generated in the vicinity the Lesser Antilles, between the two western and eastern edges of the defined control volume. Moreover, these results also indicate that the local generation of vorticity is regulated by the magnitude of the volume transport through the passages.

4.2. Temporal Variability of the Vorticity Flux

To evaluate this link between the magnitude of the volume transport and vorticity generation in more detail, we analyze the temporal variations of the vorticity fluxes. Similar to observations of Johns et al. (2002) and Rhein et al. (2005), we find highly-varying volume transports through the passages of the Lesser Antilles with a minimum modeled volume transport of 3.2 Sv in the upper 300 m of the water column and a maximum of 19.7 Sv (Figure 9a). A comparison of these volume transports to the vorticity fluxes at the western side of the Lesser Antilles confirms that there is a close relation between the magnitude of the volume transport and the magnitude

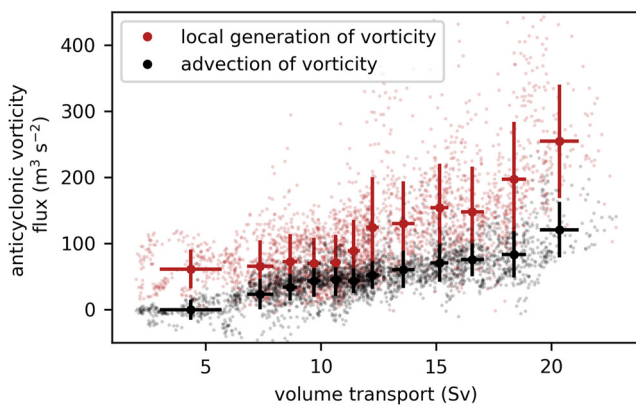


Figure 10. Relation between the total volume transport and the anticyclonic vorticity flux into the Caribbean Sea, distinguishing the local generation of vorticity (red symbols) and the advection of vorticity from the Atlantic Ocean (black dots). The local generation of vorticity is defined as the difference between the 6-hourly snapshots of the vorticity flux west and east of the Lesser Antilles (similar to gray shading in Figure 9b). The advection of vorticity corresponds to the anticyclonic vorticity flux east of the Lesser Antilles (similar to Figure 9b). The thick dots indicate average values per 250 data points, where the error bars correspond to one standard-deviation.

vorticity (red), defined as the difference between the 6-hourly snapshots west and east of the Lesser Antilles (G_{ac} in Equation 6a), also depends on the magnitude of the transport. So both the advection and generation of vorticity are proportional to the transport. Notably, the vorticity flux into the Caribbean Sea is dominated by the locally generated vorticity for all transport magnitudes.

5. Event Study of the Collision of an NBC Ring With the Lesser Antilles

Previous studies suggested that the volume transport into the Caribbean Sea is regulated by NBC rings (Mertens et al., 2009). These rings are visible as positive sea level anomalies. We extract these sea level anomalies by taking the maximum sea level anomaly ($\max(\eta - \bar{\eta})$, where $\bar{\eta}$ is the mean dynamic topography) along the yellow curve in Figure 7. During the 2-year *CS-nest* model simulation, approximately 10 rings propagate toward the Lesser Antilles. To investigate if their presence affects the generation and advection of vorticity, we study a collision of an NBC ring with the Lesser Antilles in more detail (period indicated by blue shading in Figure 9).

The start of the collision event is defined as the moment when the NBC ring passes between Tobago and Barbados (peak in sea level in Figure 9d). At that time, the volume transport into the Caribbean is already increasing (Figure 9a). This coincides with an increase of the anticyclonic and cyclonic vorticity flux on the western side of the Lesser Antilles (solid lines in Figures 9b and 9c). The end of the collision event is defined as when the anticyclonic vorticity of the NBC ring has diminished east of the Lesser Antilles. This occurs approximately 25 days later.

To determine how the presence of the NBC ring affects the fluxes of vorticity, we first describe the collision event in Section 5.1 using 6-hourly snapshots of the vorticity fields. The description starts 40 days before the collision event with snapshots from the *CS-nest* and continues to approximately 40 days after the event. Subsequently, we analyze the time-averaged vorticity fluxes of this collision in Section 5.2. A movie of this collision event containing snapshots of the *CS-nest* can be found in the Supplementary Material.

5.1. Descriptive Analysis

Vorticity snapshots of the collision event obtained from the *CS-nest* are displayed in Figure 11. A more detailed zoom of the Lesser Antilles region during the collision event can be found in Figure 2 in Supporting Information S1. On 2 May, which is approximately 40 days before the collision, two NBC rings are present in the Atlantic

of the anticyclonic and cyclonic vorticity fluxes (solid lines in Figures 9b and 9c). More specifically, the peaks in volume transport coincide with peaks in the anticyclonic and cyclonic vorticity flux into the eastern Caribbean Sea (solid line in Figures 9b and 9c). For example, during maximum inflow on 19 June, the anticyclonic vorticity flux has a maximum of $358 \text{ m}^3 \text{ s}^{-2}$, while it was much smaller on 5 October ($57 \text{ m}^3 \text{ s}^{-2}$) when the volume transport was weak (2.6 Sv, solid line in Figure 9b). The vertical advection of anticyclonic vorticity into the control volume was much smaller and varied between $-10 \text{ m}^3 \text{ s}^{-2}$ (fifth percentile) and $8.5 \text{ m}^3 \text{ s}^{-2}$ (95th percentile). The northward advection varied between $-19.7 \text{ m}^3 \text{ s}^{-2}$ (fifth percentile) and $24 \text{ m}^3 \text{ s}^{-2}$ (95th percentile). The vorticity flux east of the Lesser Antilles is at all times smaller than the flux on the western side of the islands. This indicates that anticyclonic vorticity is continuously generated at the Lesser Antilles (gray shading in Figure 9b). The same is found for the cyclonic vorticity flux, of which the magnitude also has a strong connection to the magnitude of the volume transport.

Figure 10 shows a more detailed analysis of the relation between the total volume transport through the Lesser Antilles and the generation and advection of vorticity. The contribution of advection, which is defined as the 6-hourly snapshots of vorticity flux through the eastern cross section, increases with increasing transport (black points in Figure 10). This implies that, on average, with stronger volume transport more anticyclonic vorticity is transported into the eastern Caribbean Sea. Similar to the advection, the local generation of

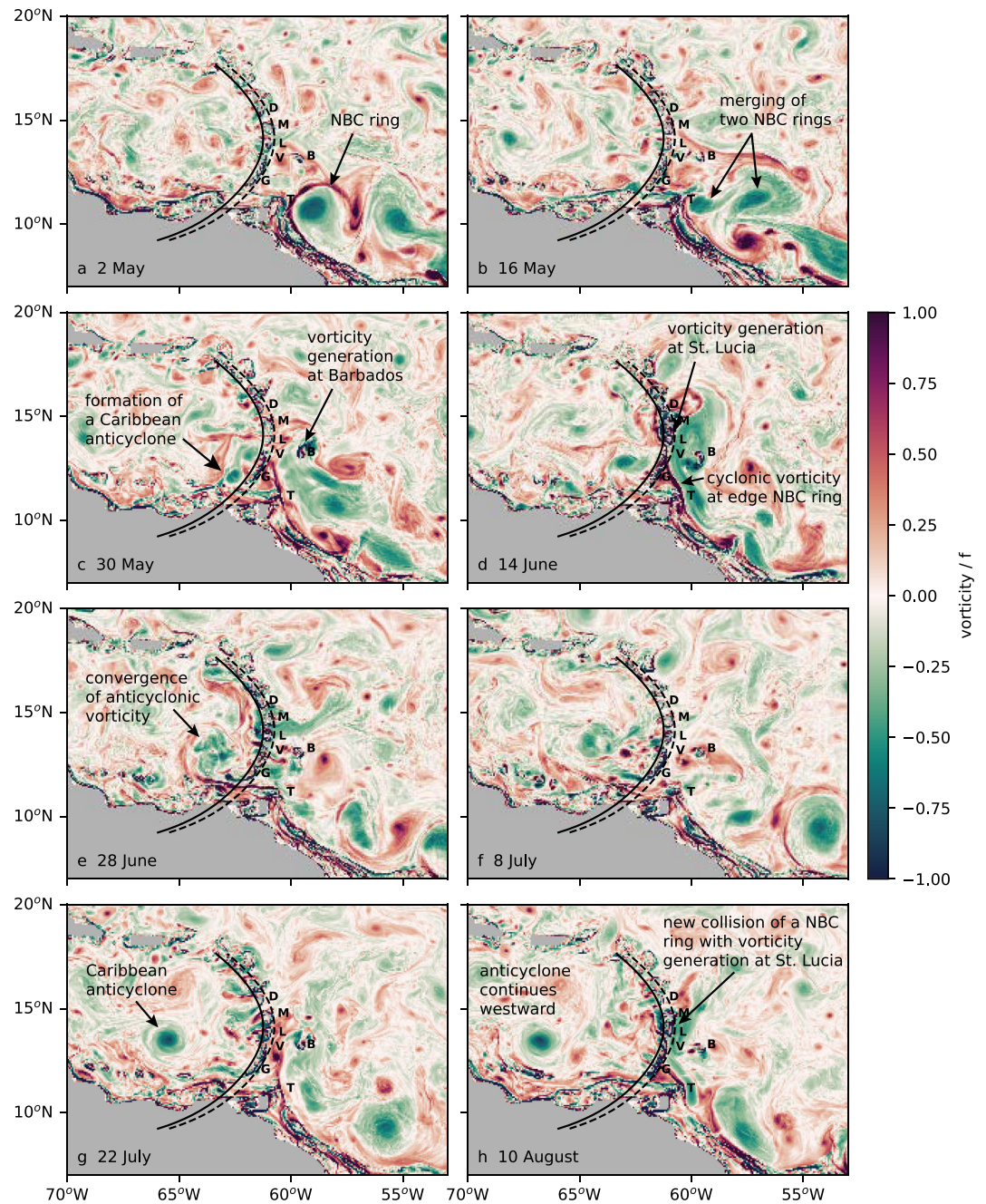


Figure 11. Vorticity averaged over the upper 300 m modeled using the *CS-nest*, scaled with the local Coriolis parameter during a collision event of an North Brazil Current (NBC) ring with the Lesser Antilles on (a) 2 May, (b) 16 May, (c) 20 May, (d) 14 June, (e) 28 June, (f) 8 July, (g) 22 July, (h) 10 August. Dashed and solid lines indicate the locations of the cross sections east and west of the Lesser Antilles, respectively. Letters are placed east of the islands to indicate their location: D = Dominica, M = Martinique, L = St. Lucia, V = St. Vincent, G = Grenada, T = Tobago, B = Barbados.

Ocean (Figure 11a). Both rings have an anticyclonic core (green shading in Figure 11), of which one has a cyclonic edge (red shading). Similar to observations of Cruz-Gómez and Vazquez (2018), we find that the NBC ring with a cyclonic edge stalls south of Barbados (B). Fourteen days later on 16 May, the two rings merge (Figure 11b). On 30 May, the merged NBC ring approaches the Lesser Antilles and passes the first ridge between Barbados (B) and Tobago (T, Figure 11c). During this passage, anticyclonic vorticity is generated near Barbados in the wake of the island. At the same time, the cyclonic edge of the NBC ring separates the anticyclonic core from the Lesser

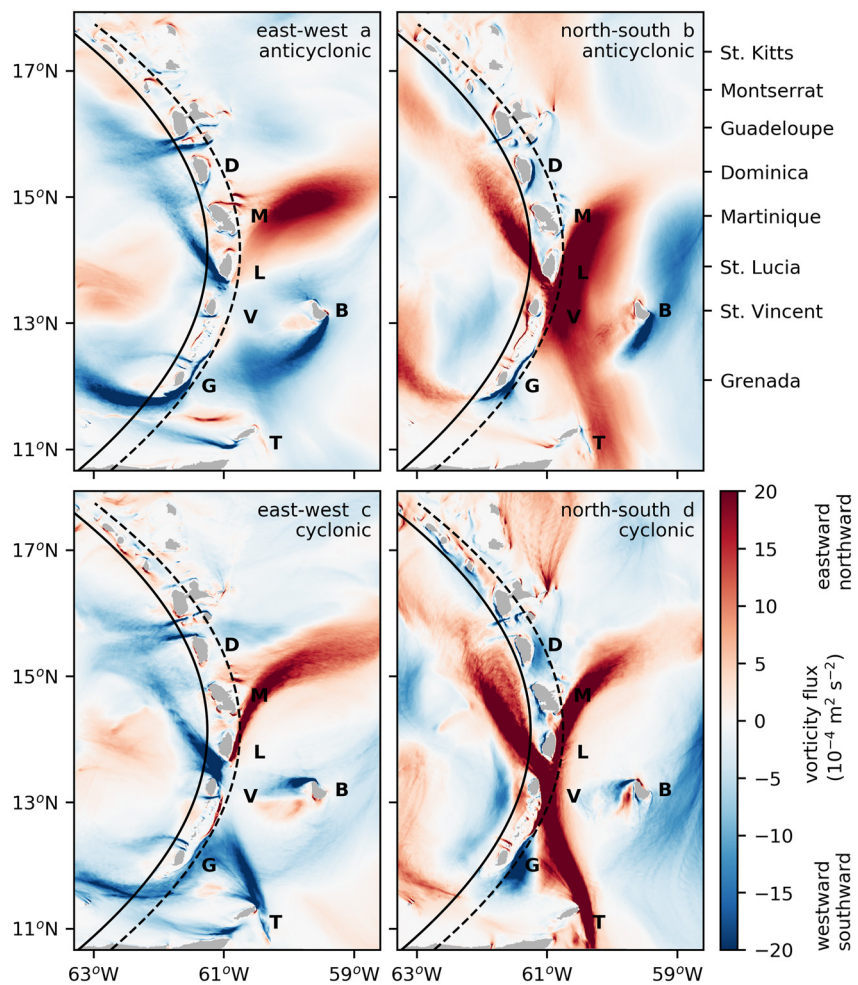


Figure 12. Directional vorticity flux integrated over the upper 300 m of the water column and averaged between 3 June and 28 June (*LA-nest*). (a, b) Anticyclonic vorticity flux in (a) eastward and (b) northward direction; (c, d) Cyclonic vorticity flux in (c) eastward and (d) northward direction. The absolute value of the vorticity is used in the computation of anticyclonic vorticity flux (Equation 6). Dashed and solid lines indicate the locations of the cross sections east and west of the Lesser Antilles, respectively. Letters are placed east of the islands to indicate their location: D = Dominica, M = Martinique, L = St. Lucia, V = St. Vincent, G = Grenada, T = Tobago, B = Barbados.

Antilles. This effect is still visible between Tobago (T) and St. Vincent (V) 14 days later on 14 June (Figure 11d). Fourteen days later, an anticyclone forms on the Caribbean side of the Lesser Antilles (Figures 11e and 11f). This anticyclone consists of merged submesoscale filaments of vorticity that can be traced back to Grenada (G, Figure 11e) and to St. Lucia (L, Figure 11d). After formation, this anticyclone propagates along the mean flow in westward direction (Figures 11g and 11h).

5.2. Vorticity Generation

The snapshots of the vorticity field highlight the two different sources of anticyclonic vorticity that flow into the eastern Caribbean Sea during the NBC ring-island collision event: advection of vorticity from the Atlantic Ocean and the local generation of vorticity near the Lesser Antilles. To analyze the contribution of these sources, we compute the time-averaged vorticity fluxes during the collision event (Figure 12). For completeness, we show the fluxes of both anticyclonic (Figures 12a and 12b) and cyclonic vorticity (Figures 12c and 12d).

The advection of anticyclonic vorticity from the NBC ring into the eastern Caribbean Sea is visible on the Atlantic side of the Lesser Antilles. This westward advection of anticyclonic vorticity from the eastern boundary of the domain toward the Caribbean is minor as, judging from the spatial pattern (blue shading in Figure 12a),

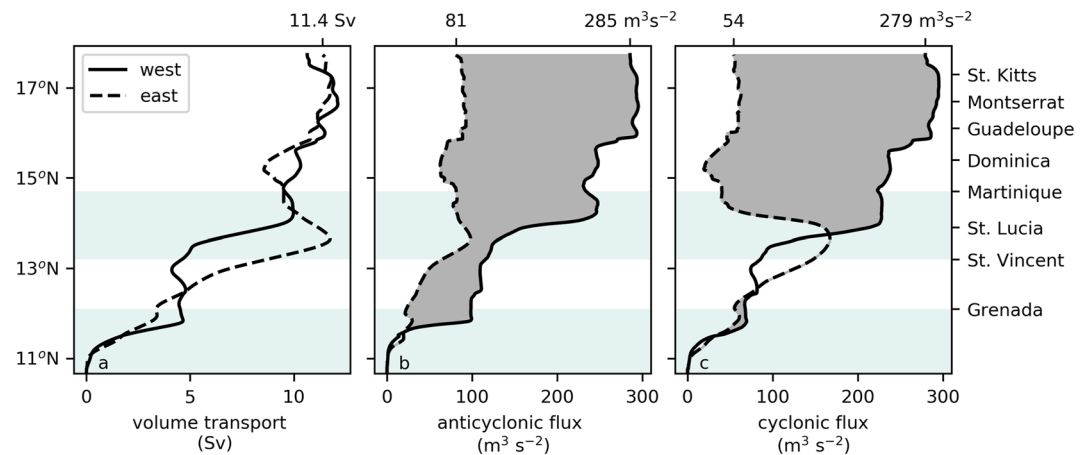


Figure 13. Same as Figure 8, but then during the collision of a North Brazil Current (NBC) ring with the Lesser Antilles (3–28 June, as simulated by the *LA-nest* configuration).

most anticyclonic vorticity appears to be generated at the islands. At the southern boundaries of Tobago (T) and Barbados (B), we find clear maximums of the flux of anticyclonic vorticity, which shows that vorticity is locally generated there. Similar to its westward advection, the northward advection of anticyclonic vorticity indicates locations with enhanced local generation of vorticity (red shading in Figure 12b). Recall that we use the absolute value of vorticity (Equation 6), which implies that positive fluxes are in northward direction for both cyclonic and anticyclonic vorticity. One of these locations is the passage south of St. Lucia (L), where also some of the anticyclonic vorticity of the NBC rings is advected. Also part of the cyclonic edge of the NBC ring is advected through this passage, which is visible by a maximum that extends from the southern boundary toward St. Lucia (L, Figures 12c and 12d). Northward of St. Lucia, it splits into an Atlantic branch and a Caribbean branch.

To quantify the relative contributions of the advection and generation of vorticity, we compute the 25-day averaged volume transport and vorticity fluxes through the previously defined cross sections during this event (Equation 6 and Figure 13). Similar to Figure 8, the fluxes were computed perpendicular to the cross section, which implies that both zonal (Figures 12a and 12c) and meridional fluxes (Figures 12b and 12d) are taken into account. Compared to the time-averaged fluxes (Figure 8), the anticyclonic and cyclonic vorticity flux into the eastern Caribbean are relatively high during the event (Figures 13b and 13c). These anomalously high fluxes of vorticity coincide with a relatively high-volume transport and are both due to increased advection of vorticity and enhanced generation of vorticity. Consequently, only 29% of the vorticity flux into the Caribbean Sea can be attributed vorticity from the Atlantic Ocean. Recall that east of the most eastern cross section also vorticity is generated at Tobago and Barbados (Figure 13). This implies that the contribution of the vorticity of NBC rings is at most 29%.

During the collision event, we obtain a similar latitudinal variation in the generation of vorticity as found in the 2-year averaged fluxes (Figures 8, Fig. 13b). Most anticyclonic vorticity is generated locally south of Grenada and near St. Lucia (light blue shading in Figure 13b). Most cyclonic vorticity is generated near St. Lucia (Figure 13c). Overall, these results show that also during the collision of an NBC ring with the Lesser Antilles the bulk of the vorticity flux into the Caribbean Sea is generated near the topography.

6. Summary, Discussion, and Conclusions

In this study, we distinguished between the local generation of vorticity near the steep topography of the Lesser Antilles island arc, which separates the Atlantic Ocean from the Caribbean Sea, and the advection of vorticity from the Atlantic Ocean into the Caribbean Sea using a high-resolution numerical model. On the Atlantic side of the Lesser Antilles, the flow is dominated by anticyclonic North Brazil Current (NBC) rings that collide with this island arc. In contrast to previous studies (Huang et al., 2021; van Westen et al., 2018), who based their analysis on the propagation of sea level anomalies, we concluded that Caribbean anticyclones are not remnants of NBC rings and that the bulk of their vorticity is locally generated near the island arc. Our model results indicate that

the vertical structure of these anticyclonic eddies is diverse. Some anticyclones have a strong baroclinic structure similar to observations of van der Boog, de Jong et al. (2019), while other anticyclones displayed stronger flow velocities below the thermocline, as was previously observed by Rudzin et al. (2017).

To separate the local generation of vorticity near the steep topography from the vorticity contained in the NBC rings, we computed the fluxes of vorticity east and west of the Lesser Antilles. This allowed us to quantify the relative contributions of the vorticity advected from the Atlantic Ocean (containing the vorticity contribution of the NBC rings) and the vorticity that is locally generated. We found that, during the 2 years of the model simulation, 67% of the anticyclonic vorticity flux is generated locally. The remaining 33% of the vorticity flux is advected from the Atlantic Ocean. The latter contribution contains both the vorticity generated locally at the easternmost islands of the Lesser Antilles (Tobago and Barbados) and the anticyclonic vorticity filaments of North Brazil Current rings that collide with the islands.

However, this does not imply that the NBC rings cannot regulate the magnitude of the vorticity contribution that enters the Caribbean Sea. We showed that the local generation of vorticity depends on the magnitude of the volume transport from the Atlantic Ocean to the Caribbean Sea and that the passages with the strongest volume transport also display the strongest local generation of vorticity. The passages south of Grenada and between St. Vincent and Martinique, which are known for their strong volume transport (Johns et al., 2002; Rhein et al., 2005), show this enhanced vorticity generation and the bulk of the locally generated vorticity originates in these regions (Figure 7). These results are supported by observations (Andrade & Barton, 2000; Richardson, 2005) that show that most Caribbean anticyclones are formed directly downstream of these passages. The transport through these passages is, in turn, regulated by the presence or absence of NBC rings (Mertens et al., 2009): Before a collision event, the NBC ring first decrease the volume transport, and then enhance it. In line with these results, we obtained strong variations in volume transport through passages of the Lesser Antilles during the collision of an NBC ring. Simultaneously, both the vorticity flux from the Atlantic Ocean and the local generation of vorticity increased. This enhanced inflow resulted in the formation of a Caribbean anticyclone downstream. While this anticyclone corroborates the existence of a connection between the presence of NBC rings and the formation of Caribbean anticyclones as was previously reported (Goni & Johns, 2001, 2003; Richardson, 2005; Rudzin et al., 2017; van Westen et al., 2018), our model results suggest that this connection is indirect, and that Caribbean anticyclones are predominantly generated in response to the increase in volume transport into the Caribbean Sea and associated local generation of vorticity near the island arc.

Overall, the results of this study show that local generation of vorticity near the steep topography of the Lesser Antilles is a crucial part in the vorticity budget of the Caribbean Sea. This vorticity can be generated by different processes. For example, vortex stretching over topography, vortex tilting near the steep boundaries, squeezing of anticyclonic vorticity through narrow passages and frictional processes can increase the vorticity. To determine the precise mechanisms responsible for the vorticity generation, a detailed analysis of the vorticity budget is an interesting direction for further research. We speculate that the bulk of the vorticity is generated by frictional processes take place in the bottom boundary layer (e.g., Dong & McWilliams, 2007; Srinivasan et al., 2017; Vic et al., 2015). Idealized modeling studies showed that these frictional processes significantly contribute to the vorticity budget through the so-called bottom stress divergence torque, which is the dominant contribution to the bottom pressure torque in models that resolve the bottom boundary layer (Jagannathan et al., 2021). In particular, the no-slip boundary condition generates horizontal and vertical shear layers in the bottom boundary layer when a flow encounters a sloping topography (Srinivasan et al., 2019). In turn, these shear layers can lead to the formation of vortices downstream by a combination of barotropic and centrifugal instabilities (Gula et al., 2015; Molemaker et al., 2015; Srinivasan et al., 2019). In this study, we showed that even in an eddy-dominated flow, the vorticity downstream of steep topography is predominantly locally generated. Therefore, this study highlights the importance of vorticity generation by means of flow-topography interactions. Because these interactions are ubiquitous in the ocean, they are expected to be important whenever currents and steep topography meet.

Appendix A: Water Masses in the Caribbean Sea

To identify whether the flow into the Caribbean Sea contains a realistic representation of the water masses, we analyze the time-averaged properties of the water masses in the model (Figure A1). Because, the Caribbean anticyclones are shallow, and the vorticity fluxes are analyzed to a depth of 300 m, we limit ourselves to the validation

of the characteristics of the upper-ocean water masses. The model contains the two distinctive water masses that are characteristic for the upper Caribbean Sea: the subsurface properties (i.e., the salinity maximum) of Subtropical Underwater (STUW) and the surface properties of Caribbean Surface Water (Morrison & Nowlin, 1982; Hernández-Guerra & Joyce, 2000, CSW). A comparison to data from the WOA2018 in the eastern Caribbean Sea (63°–66°W, 13°–17°N, Figure A1) indicates that the model underestimates the salinity of the STUW. We find a salinity maximum of $S = 36.8 \text{ g kg}^{-1}$ in the model compared to $S = 37.1 \text{ g kg}^{-1}$ in the WOA2018. This underestimation is seen in both the Atlantic Ocean and the Caribbean Sea. Taking the relatively long travel distance of STUW from its formation region in the central tropical Atlantic to the Caribbean Sea into account (Montes et al., 2016; Qu et al., 2013), this underestimation is likely the result of too much diapycnal mixing in the parent simulation.

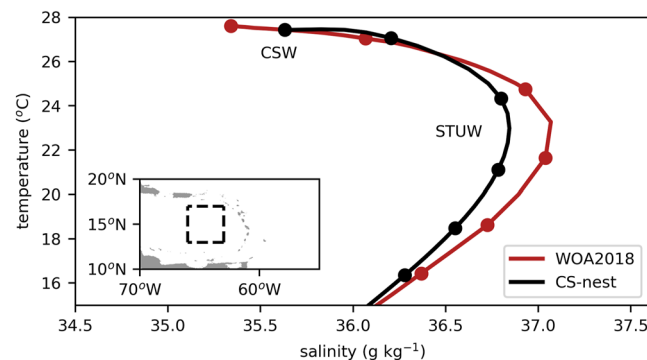


Figure A1. Temperature-Salinity diagram of the time-mean conservative temperature and absolute salinity in the eastern Caribbean Sea (63°–66°W, 13°–17°N, see dashed box in inset) for the simulations with the *CS-nest* (black) and WOA2018 (red). Dots correspond to depth levels from 0 to 250 m with intervals of 50 m. The approximate locations of Caribbean Surface Water (CSW) and Subtropical Underwater (STUW) are indicated.

In contrast, the temperature distribution of STUW is adequately modeled and the surface properties of the CSW are also well represented in the model (Figure A1). The adequate representation of these surface properties implies that the surface forcing is well captured by the model and that the model is able to represent the time-averaged temperature and salinity in this basin.

Data Availability Statement

The data used in the computations of the figures and tables are available at doi.org/10.5281/zenodo.4550460.

References

- Andersson, A., Fennig, K., Klepp, C., Bakan, S., Graßl, H., & Schulz, J. (2010). The Hamburg ocean atmosphere parameters and fluxes from satellite data—HOAPS-3. *Earth System Science Data*, 2(2), 215–234. <https://doi.org/10.5194/essd-2-215-2010>
- Andrade, C. A., & Barton, E. D. (2000). Eddy development and motion in the Caribbean Sea. *Journal of Geophysical Research*, 105(C11), 26191–26201. <https://doi.org/10.1029/2000JC000300>
- Cardoso, C., Caldeira, R. M., Relvas, P., & Stegner, A. (2020). Islands as eddy transformation and generation hotspots: Cabo Verde case study. *Progress in Oceanography*, 184, 102271. <https://doi.org/10.1016/j.poccean.2020.102271>
- Cenedese, C., Adduce, C., & Fratantoni, D. M. (2005). Laboratory experiments on mesoscale vortices interacting with two islands. *Journal of Geophysical Research*, 110, C09023. <https://doi.org/10.1029/2004JC002734>
- Centurioni, L. R., & Niiler, P. P. (2003). On the surface currents of the Caribbean Sea. *Geophysical Research Letters*, 30(6), 1279. <https://doi.org/10.1029/2002GL016231>
- Chelton, D. B., Schlax, M. G., & Samelson, R. M. (2011). Global observations of nonlinear mesoscale eddies. *Progress in Oceanography*, 91(2), 167–216. <https://doi.org/10.1016/j.poccean.2011.01.002>
- Chelton, D. B., Schlax, M. G., Samelson, R. M., & de Szoeke, R. A. (2007). Global observations of large oceanic eddies. *Geophysical Research Letters*, 34, L15606. <https://doi.org/10.1029/2007GL030812>
- Chérubin, L., & Richardson, P. (2007). Caribbean current variability and the influence of the Amazon and Orinoco freshwater plumes. *Deep Sea Research Part I: Oceanographic Research Papers*, 54(9), 1451–1473. <https://doi.org/10.1016/j.dsr.2007.04.021>
- Cruz-Gómez, R. C., & Vazquez, H. J. (2018). Interaction of North Brazil current rings with the lesser Antilles arc and Barbados island: Laboratory experiments and observations. *Environmental Fluid Mechanics*, 18(5), 1203–1226. <https://doi.org/10.1007/s10652-018-9592-x>

Acknowledgments

The work of Carine van der Boog is financed by a Delft Technology Fellowship awarded to Caroline Katsman by Delft University of Technology. This work is part of the research program ALW-Caribbean with project 858.14.061 (SCENES), which is financed by the Netherlands Organisation for Scientific Research (NWO). The research described in this paper was carried out in part at the Jet Propulsion Laboratory, California Institute of Technology, under a contract with NASA. (c) 2021 All rights reserved. US Government sponsorship is acknowledged.

- Dai, A., & Trenberth, K. E. (2002). Estimates of freshwater discharge from continents: Latitudinal and seasonal variations. *Journal of Hydrometeorology*, 3(6), 660–687. [https://doi.org/10.1175/1525-7541\(2002\)003<0660:EOFDPC>2.0.CO;2](https://doi.org/10.1175/1525-7541(2002)003<0660:EOFDPC>2.0.CO;2)
- de Boyer Montégut, C., Madec, G., Fischer, A. S., Lazar, A., & Iudicone, D. (2004). Mixed layer depth over the global ocean: An examination of profile data and a profile-based climatology. *Journal of Geophysical Research*, 109, C12003. <https://doi.org/10.1029/2004JC002378>
- Deremble, B., Dewar, W. K., & Chassignet, E. P. (2016). Vorticity dynamics near sharp topographic features. *Journal of Marine Research*, 74(6), 249–276. <https://doi.org/10.1357/002224016821744142>
- Diden, N., & Schott, F. (1993). Eddies in the North Brazil Current retroflection region observed by Geosat altimetry. *Journal of Geophysical Research*, 98(C11), 20121–20131. <https://doi.org/10.1029/93JC01184>
- Dong, C., & McWilliams, J. C. (2007). A numerical study of island wakes in the Southern California Bight. *Continental Shelf Research*, 27(9), 1233–1248. <https://doi.org/10.1016/j.csr.2007.01.016>
- Duran-Matute, M., & Fuentes, O. U. V. (2008). Passage of a barotropic vortex through a gap. *Journal of Physical Oceanography*, 38(12), 2817–2831. <https://doi.org/10.1175/2008JPO3887.1>
- Fratantoni, D. M., & Richardson, P. L. (2006). The evolution and Demise of North Brazil current rings. *Journal of Physical Oceanography*, 36(7), 1241–1264. <https://doi.org/10.1175/JPO2907.1>
- Fu, L.-L., Chelton, D. B., Le Traon, P.-Y., & Morrow, R. (2010). Eddy dynamics from satellite altimetry. *Oceanography*, 23, 14–25.
- Gaube, P., J. McGillicuddy, D., & Moulin, A. J. (2019). Mesoscale eddies modulate mixed layer depth globally. *Geophysical Research Letters*, 46, 1505–1512. <https://doi.org/10.1029/2018GL080006>
- Goni, G. J., & Johns, W. E. (2001). A census of North Brazil current rings observed from TOPEX/POSEIDON altimetry: 1992–1998. *Geophysical Research Letters*, 28(1), 1–4. <https://doi.org/10.1029/2000GL011717>
- Goni, G. J., & Johns, W. E. (2003). Synoptic study of warm rings in the North Brazil Current retroflection region using satellite altimetry. *Elsevier Oceanography Series*, 68, 335–356. [https://doi.org/10.1016/S0422-9894\(03\)80153-8](https://doi.org/10.1016/S0422-9894(03)80153-8)
- Gula, J., Molemaker, M. J., & McWilliams, J. C. (2015). Topographic vorticity generation, submesoscale instability and vortex street formation in the Gulf Stream. *Geophysical Research Letters*, 42, 4054–4062. <https://doi.org/10.1002/2015GL063731>
- Hernández-Guerra, A., & Joyce, T. M. (2000). Water masses and circulation in the surface layers of the Caribbean at 66W. *Geophysical Research Letters*, 27(21), 3497–3500. <https://doi.org/10.1029/1999GL011230>
- Huang, M., Liang, X., Zhu, Y., Liu, Y., & Weisberg, R. H. (2021). Eddies connect the tropical Atlantic Ocean and the Gulf of Mexico. *Geophysical Research Letters*, 48, e2020GL091277. <https://doi.org/10.1029/2020GL091277>
- Itoh, S., & Yasuda, I. (2010). Characteristics of mesoscale eddies in the Kuroshio-Oyashio extension region detected from the distribution of the sea surface height anomaly. *Journal of Physical Oceanography*, 40(5), 1018–1034. <https://doi.org/10.1175/2009JPO4265.1>
- Jagannathan, A., Srinivasan, K., McWilliams, J. C., Molemaker, M. J., & Stewart, A. L. (2021). Boundary layer-mediated vorticity generation in currents over sloping bathymetry. *Journal of Physical Oceanography*, 1757–1778. <https://doi.org/10.1175/JPO-D-20-0253.1>
- Jiménez, B., Sangrà, P., & Mason, E. (2008). A numerical study of the relative importance of wind and topographic forcing on oceanic eddy shedding by tall, deep water islands. *Ocean Modelling*, 22(3), 146–157. <https://doi.org/10.1016/j.ocemod.2008.02.004>
- Jochumsen, K., Rhein, M., Hüttl-Kabus, S., & Böning, C. W. (2010). On the propagation and decay of North Brazil Current rings. *Journal of Geophysical Research*, 115, C10004. <https://doi.org/10.1029/2009JC006042>
- Johns, W. E., Townsend, T. L., Fratantoni, D. M., & Wilson, W. D. (2002). On the Atlantic inflow to the Caribbean Sea. *Deep-Sea Research Part I: Oceanographic Research Papers*, 49(2), 211–243. [https://doi.org/10.1016/S0967-0637\(01\)00041-3](https://doi.org/10.1016/S0967-0637(01)00041-3)
- Johnston, T. S., Schönau, M. C., Paluszkiwicz, T., MacKinnon, J. A., Arbic, B. K., Colin, P. L., & Zeiden, K. L. (2019). Flow encountering steep topography (FLEAT). *Oceanography*, 32(4), 10–21. <https://doi.org/10.2307/26845634>
- Jouanno, J., Sheinbaum, J., Barnier, B., Marc Molines, J., & Candela, J. (2012). Seasonal and interannual modulation of the eddy kinetic energy in the Caribbean Sea. *Journal of Physical Oceanography*, 42(11), 2015–2055. <https://doi.org/10.1175/JPO-D-12-048.1>
- Jouanno, J., Sheinbaum, J., Barnier, B., & Molines, J. (2009). The mesoscale variability in the Caribbean Sea. Part II: Energy sources. *Ocean Modelling*, 26(3–4), 226–239. <https://doi.org/10.1016/j.ocemod.2008.10.006>
- Kirchner, K., Rhein, M., Mertens, C., Böning, C. W., & Hüttl, S. (2008). Observed and modeled meridional overturning circulation related flow into the Caribbean. *Journal of Geophysical Research*, 113, C03028. <https://doi.org/10.1029/2007JC004320>
- Large, W. G., McWilliams, J. C., & Doney, S. C. (1994). Oceanic vertical mixing: A review and a model with a nonlocal boundary layer parameterization. *Reviews of Geophysics*, 32(4), 363. <https://doi.org/10.1029/94RG01872>
- Large, W. G., & Yeager, S. G. (2009). The global climatology of an interannually varying air-sea flux data set. *Climate Dynamics*, 33(2–3), 341–364. <https://doi.org/10.1007/s00382-008-0441-3>
- Lemarié, F., Kurian, J., Shchepetkin, A. F., Jeroen Molemaker, M., Colas, F., & McWilliams, J. C. (2012). Are there inescapable issues prohibiting the use of terrain-following coordinates in climate models? *Ocean Modelling*, 42, 57–79. <https://doi.org/10.1016/j.ocemod.2011.11.007>
- Locarnini, R. A., Mishonov, A. V., Baranova, O. K., Boyer, T. P., Zweng, M. M., Garcia, H. E., et al. (2019). World Ocean Atlas 2018, volume 1: Temperature (Tech. Rep. Mishonov Technical Ed.; NOAA Atlas NESDIS 81).
- Mason, E., Colas, F., Molemaker, J., Shchepetkin, A. F., Troupin, C., McWilliams, J. C., & Sangrà, P. (2011). Seasonal variability of the canary current: A numerical study. *Journal of Geophysical Research*, 116, C06001. <https://doi.org/10.1029/2010JC006665>
- Mason, E., Molemaker, J., Shchepetkin, A. F., Colas, F., McWilliams, J. C., & Sangrà, P. (2010). Procedures for offline grid nesting in regional ocean models. *Ocean Modelling*, 35(1–2), 1–15. <https://doi.org/10.1016/j.ocemod.2010.05.007>
- Mason, E., Pascual, A., & McWilliams, J. C. (2014). A new sea surface height–based code for oceanic mesoscale eddy tracking. *Journal of Atmospheric and Oceanic Technology*, 31(5), 1181–1188. <https://doi.org/10.1175/JTECH-D-14-00019.1>
- McDougall, T. J., & Barker, P. M. (2011). Getting started with TEOS-10 and the Gibbs Seawater (GSW) oceanographic toolbox. *SCOR/IAPSO WG*, 127, 1–28.
- Mélice, J.-L., & Arnault, S. (2017). Investigation of the intra-annual variability of the north equatorial countercurrent/north Brazil current eddies and of the instability waves of the north tropical Atlantic Ocean using satellite altimetry and empirical mode decomposition. *Journal of Atmospheric and Oceanic Technology*, 34(10), 2295–2310. doi <https://doi.org/10.1175/JTECH-D-17-0032.1>
- Mertens, C., Rhein, M., Walter, M., & Kirchner, K. (2009). Modulation of the inflow into the Caribbean Sea by north Brazil current rings. *Deep Sea Research Part I: Oceanographic Research Papers*, 56(7), 1057–1076. <https://doi.org/10.1016/j.dsr.2009.03.002>
- Mignot, J., de Boyer Montégut, C., Lazar, A., & Cravatte, S. (2007). Control of salinity on the mixed layer depth in the World Ocean: 2. Tropical areas. *Journal of Geophysical Research*, 112, C10010. <https://doi.org/10.1029/2006JC003954>
- Mignot, J., Lazar, A., & Lacarra, M. (2012). On the formation of barrier layers and associated vertical temperature inversions: A focus on the northwestern tropical Atlantic. *Journal of Geophysical Research*, 117, C02010. <https://doi.org/10.1029/2011JC007435>
- Molemaker, M. J., McWilliams, J. C., & Dewar, W. K. (2015). Submesoscale instability and generation of mesoscale Anticyclones near a separation of the California undercurrent. *Journal of Physical Oceanography*, 45(3), 613–629. <https://doi.org/10.1175/JPO-D-13-0225.1>

- Montes, E., Muller-Karger, F. E., Cianca, A., Lomas, M. W., Lorenzoni, L., & Habtes, S. (2016). Decadal variability in the oxygen inventory of North Atlantic subtropical underwater captured by sustained, long-term oceanographic time series observations. *Global Biogeochemical Cycles*, *30*, 460–478. <https://doi.org/10.1002/2015GB005183>
- Morrison, J. M., & Nowlin, W. D. (1982). General distribution of water masses within the eastern Caribbean Sea during the winter of 1972 and fall of 1973. *Journal of Geophysical Research*, *87*(C6), 4207–4229. <https://doi.org/10.1029/JC087iC06p04207>
- Prants, S., Lobanov, V., Budyansky, M., & Uleysky, M. (2016). Lagrangian analysis of formation, structure, evolution and splitting of anticyclonic Kuril eddies. *Deep Sea Research Part I: Oceanographic Research Papers*, *109*, 61–75. <https://doi.org/10.1016/j.dsr.2016.01.003>
- Qu, T., Gao, S., & Fukumori, I. (2013). Formation of salinity maximum water and its contribution to the overturning circulation in the North Atlantic as revealed by a global general circulation model. *Journal of Geophysical Research: Oceans*, *118*, 1982–1994. <https://doi.org/10.1002/jgrc.20152>
- Rabinovich, A. B., Thomson, R. E., & Bograd, S. J. (2002). Drifter observations of anticyclonic eddies near Bussol' strait, the Kuril islands. *Journal of Oceanography*, *58*(5), 661–671. <https://doi.org/10.1023/A:1022890222516>
- Rhein, M., Kirchner, K., Mertens, C., Steinfeldt, R., Walter, M., & Fleischmann-Wischnath, U. (2005). Transport of South Atlantic water through the passages south of Guadeloupe and across 16N, 2000–2004. *Deep Sea Research Part I: Oceanographic Research Papers*, *52*(12), 2234–2249. <https://doi.org/10.1016/j.dsr.2005.08.003>
- Richardson, P. L. (1983). Eddy kinetic energy in the North Atlantic from surface drifters. *Journal of Geophysical Research*, *88*(C7), 4355–4367. <https://doi.org/10.1029/JC088iC07p04355>
- Richardson, P. L. (2005). Caribbean Current and eddies as observed by surface drifters. *Deep Sea Research Part II: Topical Studies in Oceanography*, *52*(3–4), 429–463. <https://doi.org/10.1016/j.dsr2.2004.11.001>
- Richardson, P. L., & Tychensky, A. (1998). Meddy trajectories in the Canary Basin measured during the SEMAPHORE experiment, 1993–1995. *Journal of Geophysical Research*, *103*(C11), 25029–25045. <https://doi.org/10.1029/97JC02579>
- Risien, C. M., & Chelton, D. B. (2008). A global climatology of surface wind and wind stress fields from Eight Years of QuikSCAT scatterometer data. *Journal of Physical Oceanography*, *38*(11), 2379–2413. <https://doi.org/10.1175/2008JPO3881.1>
- Rudzin, J. E., Shay, L. K., Jaimes, B., & Brewster, J. K. (2017). Upper ocean observations in eastern Caribbean Sea reveal barrier layer within a warm core eddy. *Journal of Geophysical Research: Oceans*, *122*, 1057–1071. <https://doi.org/10.1002/2016JC012339>
- Shchepetkin, A. F. (2015). An adaptive, Courant-number-dependent implicit scheme for vertical advection in oceanic modeling. *Ocean Modelling*, *91*, 38–69. <https://doi.org/10.1016/j.ocemod.2015.03.006>
- Shchepetkin, A. F., & McWilliams, J. C. (2003). A method for computing horizontal pressure-gradient force in an oceanic model with a nonaligned vertical coordinate. *Journal of Geophysical Research*, *108*(C3), 3090. <https://doi.org/10.1029/2001JC001047>
- Shchepetkin, A. F., & McWilliams, J. C. (2005). The regional oceanic modeling system (ROMS): A split-explicit, free-surface, topography-following-coordinate oceanic model. *Ocean Modelling*, *9*(4), 347–404. <https://doi.org/10.1016/j.ocemod.2004.08.002>
- Shchepetkin, A. F., & McWilliams, J. C. (2011). Accurate Boussinesq oceanic modeling with a practical, “Stiffened” equation of state. *Ocean Modelling*, *38*(1–2), 41–70. <https://doi.org/10.1016/j.ocemod.2011.01.010>
- Shi, C., & Nof, D. (1994). The destruction of lenses and generation of Wodons. *Journal of Physical Oceanography*, *24*(6), 1120–1136. [https://doi.org/10.1175/1520-0485\(1994\)024<1120:TDOLAG>2.0.CO;2](https://doi.org/10.1175/1520-0485(1994)024<1120:TDOLAG>2.0.CO;2)
- Simmons, H. L., & Nof, D. (2002). The squeezing of eddies through gaps. *Journal of Physical Oceanography*, *32*(1), 314–335. [https://doi.org/10.1175/1520-0485\(2002\)032<0314:TSOETG>2.0.CO;2](https://doi.org/10.1175/1520-0485(2002)032<0314:TSOETG>2.0.CO;2)
- Srinivasan, K., McWilliams, J. C., Molemaker, M. J., & Barkan, R. (2019). Submesoscale vortical wakes in the lee of topography. *Journal of Physical Oceanography*, *49*(7), 1949–1971. <https://doi.org/10.1175/JPO-D-18-0042.1>
- Srinivasan, K., McWilliams, J. C., Renault, L., Hristova, H. G., Molemaker, J., & Kessler, W. S. (2017). Topographic and mixed layer submesoscale currents in the near-surface Southwestern tropical Pacific. *Journal of Physical Oceanography*, *47*(6), 1221–1242. <https://doi.org/10.1175/JPO-D-16-0216.1>
- Tanabe, A., & Cenedese, C. (2008). Laboratory experiments on mesoscale vortices colliding with an island chain. *Journal of Geophysical Research*, *113*, C04022. <https://doi.org/10.1029/2007JC004322>
- van der Boog, C. G., de Jong, M. F., Scheidat, M., Leopold, M. F., Geelhoed, S. C. V., Schulz, K., et al. (2019). Hydrographic and Biological survey of a surface-intensified anticyclonic eddy in the Caribbean Sea. *Journal of Geophysical Research: Oceans*, *124*, 6235–6251. <https://doi.org/10.1029/2018JC014877>
- van der Boog, C. G., Pietrzak, J. D., Dijkstra, H. A., Brüggemann, N., van Westen, R. M., James, R. K., et al. (2019). The impact of upwelling on the intensification of anticyclonic ocean eddies in the Caribbean Sea. *Ocean Science*, *15*(6), 1419–1437. <https://doi.org/10.5194/os-15-1419-2019>
- van Westen, R. M., Dijkstra, H. A., Klees, R., Riva, R. E. M., Slobbe, D. C., van der Boog, C. G., et al. (2018). Mechanisms of the 40–70 day variability in the Yucatan Channel volume transport. *Journal of Geophysical Research: Oceans*, *123*, 1286–1300. <https://doi.org/10.1002/2017JC013580>
- Vic, C., Roulet, G., Capet, X., Carton, X., Molemaker, M. J., & Gula, J. (2015). Eddy-topography interactions and the fate of the Persian Gulf outflow. *Journal of Geophysical Research: Oceans*, *120*, 6700–6717. <https://doi.org/10.1002/2015JC011033>
- Wunsch, C. (1999). Where do ocean eddy heat fluxes matter? *Journal of Geophysical Research*, *104*(C6), 13235–13249. <https://doi.org/10.1029/1999JC900062>
- Zweng, M. M., Reagan, J. R., Seidov, D., Boyer, T. P., Locarnini, R. A., Garcia, H. E., et al. (2019). World Ocean Atlas 2018, volume 2: Salinity (Tech. Rep. Mishonov Technical Ed.; NOAA Atlas NESDIS 82).